

An Extra Low-Mass Harmonic Radar Transponder for Insect Tracking Applications

Ramin Ala¹, Chris D. Rouse¹, Member, IEEE, and Bruce G. Colpitts, Senior Member, IEEE

Abstract—The design, construction, and performance of a harmonic radar transponder with a total mass of less than 500 μg is presented. The transponder is intended for insect tracking applications and consists of very fine wire and a small Schottky diode. It is designed for fundamental and harmonic frequencies of 10 GHz and 20 GHz, respectively. Compared to existing harmonic radar transponders, this transponder is easy to construct because the loop inductor can be implemented with a simple bend in the dipole conductor without degrading performance. Through careful design optimization, the conversion loss of the transponder is not impacted by the measures taken to minimize its mass. The expected harmonic power versus the transmitted power is estimated based on the link analysis between the transmitter and receiver of the radar, with the link analysis itself being performed via calculation, harmonic balance simulation, and full-wave simulation. The link analysis simulation predicted a received power of -66.4 dBm for a transmitted power of $+22 \text{ dBm}$ and a range of 2.4 m. The measured received power level at the harmonic frequency, obtained from the broadside of the transponder in an anechoic test chamber, is approximately -70 dBm , which agrees well with the link analysis. Simulated and measured transponder radiation patterns are also compared and show good agreement. Low-mass transponders such as this enable tracking of smaller insects without reducing their lifespan or compromising their ability to fly at natural altitudes and ranges.

Index Terms—Antenna measurements, biological radar applications, harmonic radar, miniaturized transponders, secondary radar systems.

I. INTRODUCTION

HARMONIC radar is a type of radar in which the harmonics of a transmitted signal are detected. Semiconductor elements, such as diodes, exhibit nonlinear behavior that produces harmonics of the excitation signal. This enables the detection and tracking of objects that would otherwise be indistinguishable from background clutter [1] and can be achieved with a relatively straightforward system architecture that does not require complex signal processing, as described in [2].

Radio transmitters are getting smaller and offer much better performance than radar solutions. As a result, harmonic radar is best suited to applications that involve animals and insects that are far too small for even state-of-the-art radio

Manuscript received 1 February 2023; revised 6 April 2023 and 26 May 2023; accepted 5 June 2023. Date of publication 14 June 2023; date of current version 27 June 2023. This work was supported in part by the Natural Sciences and Engineering Research Council of Canada (NSERC) Discovery Grants. (*Corresponding author: Ramin Ala.*)

The authors are with the Department of Electrical and Computer Engineering, University of New Brunswick, Fredericton, NB E3B 5A3, Canada (e-mail: ramin.ala@unb.ca).

Digital Object Identifier 10.1109/TRS.2023.3286270

transmitters. In the case of insects, the transponder must have an extremely low mass so as not to significantly affect their behavior and mobility [3]. The maximum mass that insects can carry depends on the season because during periods of high activity, their body mass tends to decrease, thus reducing their carrying capacity [4]. Optimal transponder design involves striking a balance between low mass, high fundamental-to-harmonic conversion efficiency, and ease of fabrication.

Existing harmonic radar transponders have a mass of approximately 1 mg and higher. Capaldi reported a transponder mass of 800 μg using a dipole and diode structure, which was used to track honeybees within a range of 700 m [5]. Although the information needed to assess transponder efficiency, e.g., the transmitted power and frequency, was not provided, the achieved mass is impressive. The same mass of 800 μg was achieved by connecting 8 cm of the super elastic nitinol wire to a Schottky diode using UV-activated adhesive. The resulting transponder was light enough to mount on Tephritis fruit flies [6]. A mass of 800 μg was also achieved for a 9.41 GHz transponder using AWG#42 wire and a relatively bulky diode [7]. In [8], a transponder mass of approximately 3 mg was achieved with a similar structure but thicker wire. A more complicated structure consisting of a patch antenna printed on a substrate and with a mass of 20 mg was presented in [9] for tracking bees. In [10] a printed bow-tie antenna was selected for a better matching to the diode impedance, resulting in a 20 mg transponder for snail tracking. Milanesio et al. combined two dipoles and diodes in a cross configuration to make a dual-polarized transponder that weighs approximately 12 mg [11]; this was estimated from the length, thickness, and material of the wire, as well as the mass of the diode, which is summarized in [12].

Developing a detailed model for the transponder enables both structural and performance optimization. A key performance metric is the ratio of re-radiated power density at the harmonic frequency to the incident power density at the fundamental. This depends on the antenna impedance and electrical characteristics of the diode, the latter of which are typically summarized in the corresponding SPICE model. Rasilainen et al. derived an analytical equation using equivalent circuits for the diode and antenna that yields the harmonic response in terms of the transponder antenna's received power [13]. In another work, a printed transponder equipped with a matching circuit was analytically modeled to derive the conversion efficiency from the fundamental frequency (f_0) to the second-harmonic frequency ($f_h = 2 f_0$), defined as power at f_h divide by power at f_0 . Numerical results were

also compared with harmonic balance simulations performed in PathWave Advanced Design System (ADS) [14]. In [15], Lavrenko derived an equation to relate the transponder output current in terms of a voltage source as an input signal. The resulting exponential function can then be explicitly solved in both the small- and large-signal regimes using the Lambert function. A simplified approach that considers the Schottky diode as a complex load is presented in [16], and the transponder conversion efficiency is expressed in terms of dipole and diode impedances. The effect of the dipole arm ratio and wire thickness on the impedance, as well as the bending of the arms on the radiation pattern, were examined in [17] by full-wave simulation.

In practice, the orientation of the transponder relative to the incident electromagnetic wave is unknown, which raises the need for acquiring the radiation pattern. However, due to the lack of a measurement port, conventional radiation pattern measurement methods are not applicable to the transponder. An alternative technique based on intermodulation response can be derived from a similar method used to measure the radiation patterns of RFID transponders [18]. This technique was suggested by Rasilainen to measure the individual radiation patterns of a transponder at the fundamental and harmonic frequencies [19].

In this paper, the design and performance of an extra low-mass transponder is presented. Despite efficiency issues, the simple configuration of a dipole and diode provides the lowest mass. This structure was studied experimentally at both S- and X-band with the transmitter output powers of 3 W and 10 W, respectively [20]. Here, the transponder consists of AWG#44 wire and a low-barrier Schottky diode with a footprint of 0201. Its performance is optimized by selecting a diode with low junction capacitance and parasitic inductance as well as optimizing the dipole length for a better impedance match. Table I summarizes the specifications of some harmonic transponders including their antenna structure, fundamental frequency, and total mass, along with proposed transponder, which exhibits the lowest mass while maintaining low conversion loss. Comparing the RF performance of the proposed transponder with a similar structure in this table reveals that the reduction in mass has not compromised its RF performance. In [8], a harmonic cross-section of 40 mm^2 was obtained. Comparing with the ideal harmonic cross-section of 320 mm^2 yields an estimated conversion loss of roughly 9 dB; however, it is important to note that the antenna gain at the harmonic frequency was assumed to be +3.8 dBi in [8], whereas in this paper the broadside antenna gain at the harmonic frequency is found via simulation to be -0.45 dBi. Combined with a broadside antenna gain at the fundamental frequency of approximately +2.5 dBi and the conversion loss of 4.5 dB found here, our tag exhibits a harmonic cross-section of approximately 46 mm^2 —a slight improvement in harmonic cross-section and a significant reduction in mass. The transponder model and design are described in Section II. In Section III, transponder performance is estimated by a link analysis that accounts for all power losses and gains, considering a specific distance and transmitted power. Section IV presents measurements performed in an anechoic test chamber to determine the received harmonic amplitude and tag

TABLE I
COMPARING SOME HARMONIC TRANSPONDERS

Design	Antenna structure	f_0	Mass
[5, 6]	dipole	Not Specified	$800 \mu\text{g}$
[7]	dipole	9.41 GHz	$800 \mu\text{g}$
[8]	dipole	9.41 GHz	3 mg
[9]	microstrip patch	9.4 GHz	20 mg
[11]	cross dipoles	9.41 GHz	12 mg
This Work	dipole	10 GHz	$500 \mu\text{g}$

radiation pattern. For validation purposes, measurements were performed under similar conditions to those of the link analysis simulations. Finally, Section V offers concluding remarks.

II. TRANSPONDER MODEL AND DESIGN

The design of the transponder's antenna requires simultaneous consideration of several factors, including the characteristics of the attached diode, desired radiation pattern(s), acceptable degree of complexity, and total mass. If mass reduction is the priority, the best option is a dipole with a loop that works as both a DC path and a simple matching structure. The antenna should be conjugate matched to the diode at both the fundamental and harmonic frequencies for maximum power transfer between the antenna and diode. This reduces the conversion loss, which is defined as the ratio of available power at f_0 to re-radiated power at f_h .

The impedance of a Schottky diode at a given frequency is mainly determined by its junction capacitance, dynamic resistance, and parasitic or package elements. Therefore, each diode performs best with a specifically designed antenna, and this multi-factor design process does not have a unique solution [21]. Since the harmonic radar transponder is a non-linear device, impedance matching solutions must consider the voltage driving the diode. Generally, the voltage corresponding to the maximum radar range is considered to ensure the transponder works well at the lowest incident power density.

Another consideration in antenna design is its radiation pattern, which, for a dipole, is largely governed by its length. A longer dipole has a higher broadside gain but lower 3 dB beamwidth. Table II shows the radiation pattern on a logarithmic scale at the fundamental and harmonic frequencies, f_0 and f_h , in terms of the dipole's electrical length at f_0 . The harmonic radar range equation generally has a common term as the product of gain at the fundamental and harmonic frequencies [22], [23]. Therefore, the sum of patterns at f_0 and f_h on the logarithmic scale can be taken to represent the total radiation pattern of the transponder and is shown in the rightmost column of the table. If the antenna length exceeds approximately $0.55\lambda_0$, side lobes appear at the harmonic frequency, and the total pattern loses the traditional donut shape. These side lobes make the transponder more detectable when the radar and transponder are at significantly different heights, e.g., if the radar is mounted on a drone. When the electrical length approaches λ_0 , a null is observed in the broadside direction of total pattern, which is generally undesired. The designed transponder in this paper measures approximately $0.7\lambda_0$, i.e., each arm is approximately $0.35\lambda_0$, which exhibits acceptable matching with the selected diode.

TABLE II
GENERAL SHAPE OF RADIATION PATTERN IN TERMS OF DIPOLE LENGTH

Dipole length at f_0	Pattern at f_0	Pattern at f_h	Total pattern
$L < 0.55 \lambda_0$			
$0.55 \lambda_0 < L < 0.85 \lambda_0$			
$0.85 \lambda_0 < L < 1.1 \lambda_0$			

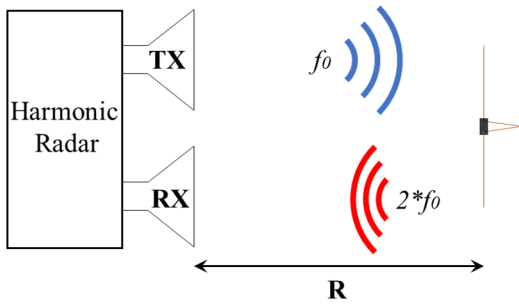


Fig. 1. Diagram of a typical harmonic radar link.

With this length of dipole, side lobes are expected at f_h and in the total radiation patterns.

The length of the loop providing a DC short across the diode in the design requires careful consideration. Simulation results indicate that increasing its length increases its inductance at both the f_0 and f_h . However, surpassing a certain threshold length result in a capacitive impedance, leading to a notable impact on conversion loss. In this case, a length between 2 to 3 mm keeps the conversion loss within an acceptable range. Similar findings have been reported in [24].

III. LINK ANALYSIS FOR A HARMONIC RADAR SYSTEM

The typical method for calculating received versus transmitted power in a telecommunication link is the link analysis, which accounts for all the power gains and losses that the signal experiences. A diagram illustrating a typical harmonic radar link is shown in Fig. 1. Contrary to a conventional radar, a harmonic radar link involves two harmonically related frequencies in the forward and return path, which means different gains and aperture areas for the radar antennas and transponder. As the conventional radar cross-section concept is not applicable in this case, the attenuation associated with the transponder can be estimated in simulation.

The available power at the transponder antenna terminals, P_a , is given by

$$P_a = S A_e \quad (1)$$

where S is the incident power density and A_e is the effective area of the transponder at f_0 , which is in turn given by

$$A_e = \frac{\lambda_0^2}{4\pi} G_0 \quad (2)$$

where G_0 is the gain of the transponder antenna at f_0 . P_a will only be delivered to the diode under perfect conjugate matching conditions. In practice, the power delivered to the diode, referred to as the ‘received power’ and denoted by P_r , is given by

$$P_r = P_a \frac{4R_d R_a}{(R_d + R_a)^2 + (X_d + X_a)^2} \quad (3)$$

where R_d and X_d are the resistance and reactance presented by the diode at f_0 , respectively; and R_d and X_d are the resistance and reactance presented by the antenna at f_0 , respectively. Note that the antenna consists of the combination of the dipole and loop in this case.

Since the behavior of a harmonic radar transponder depends upon the incident power density, a specific transmitted power and range are considered for simulation purposes. A range of $R = 2.4$ m fits within the anechoic test chamber used for experimental validation while ensuring the transponder is in the far-field region of both the transmit (TX) and receive (RX) antennas. Consider the transponder at a range of $R = 2.4$ m from a harmonic radar system with a +22 dBm transmitted power and transmit and receive antenna gains of 15.8 dBi at $f_0 = 10$ GHz and 24.5 dBi at $f_h = 20$ GHz, respectively. This pair of frequencies was primarily selected based on practical considerations, such as the available TX and RX hardware, e.g., antennas and harmonic rejection low pass filters. Working at higher frequencies is advantageous when building low-mass transponders with low conversion loss, but achieving higher peak powers is challenging at higher frequencies. Since the overall concept will remain the same, the frequency pair can be adjusted based on the table of frequency allocations in the location of use.

In the link analysis, the transponder gains at f_0 and f_h are needed to determine the amount of power collected at f_0 and reradiated at f_h . Reflection losses due to impedance mismatches are considered separately, and the transponder is assumed to be polarization-aligned with both radar antennas, i.e., polarization mismatch is neglected. The gain pattern was simulated using CST Studio Suite and resulted in a gain pattern similar to the middle row of Table II. In the following calculations, the broadside gain of the transponder is considered, which is +2.5 dBi at f_0 and -0.45 dBi at f_h . The reason for a relatively low gain at f_h is the existence of side lobes in the radiation pattern due to the length of transponder, which is longer than $0.5\lambda_0$. This directs a part of the energy to these lobes.

The available power at the transponder antenna terminals, attenuated by an impedance mismatch between the dipole and diode, yields the transponder’s received power. An equivalent circuit for the antenna is needed to derive this value, which

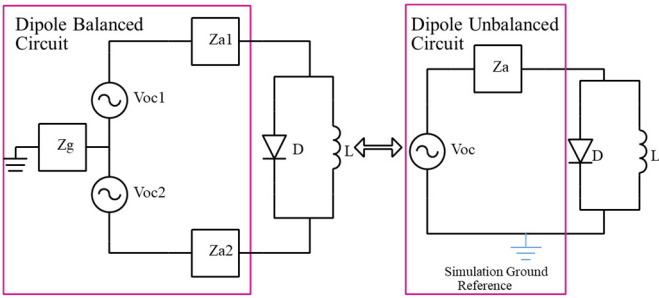


Fig. 2. Balanced and unbalanced equivalent circuits for transponder.

could be balanced or unbalanced as shown in Fig. 2. Considering the symmetry of dipole, for a very large value of Z_g in the balanced circuit, ground currents can be neglected, and V_{oc1} and V_{oc2} as well as Z_{a1} and Z_{a2} are in series. Thus,

$$\begin{cases} V_{oc} = V_{oc1} + V_{oc2} \\ Z_a = Z_{a1} + Z_{a2} \end{cases} \quad (4)$$

and the circuits can be used interchangeably.

An S-parameter analysis based on the ADS schematic shown in Fig. 3(a) provides the associated reflection coefficient. The SPICE model of the diode, including package elements, is driven by a frequency-dependent port exhibiting the impedance of the dipole and loop at both f_0 and f_h . Fig. 3(b) shows the magnitude of the reflection coefficient in dB between the MA4E2501L-1290 diode and the discussed dipole antenna. Good matching (-12.5 dB) is observed at f_0 . With the antenna impedance of $Z_a(f_0) = 4.46 + j84 \Omega$ and diode impedance of $Z_d(f_0) = 7.25 - j84.28 \Omega$, evaluation of (3) yields a ratio of 0.943 for P_r over P_a , which translates to a mismatch loss of 0.25 dB.

The next step in the link analysis is finding the amplitude of current at the harmonic frequency using a harmonic balance simulation, as shown by the ADS schematic in Fig. 4(a). An unbalanced copy of the antenna impedance derived from full-wave analysis in CST Studio Suite is in series with the diode, and the circuit is driven by an open circuit voltage source, V_{oc} , which can be expressed as [8] and [13]

$$V_{oc} = \sqrt{8R_a P_a}. \quad (5)$$

Considering the transmitter power and its antenna gain, the distance between transmitter and transponder, and the transponder's effective aperture, the available power would be $P_a = 10.71 \mu\text{W}$ or -19.7 dBm . With $R_a = 4.46 \Omega$, (5) yields $V_{oc} = 19.55 \text{ mV}$. The harmonic balance simulation results are depicted by Fig. 4(b) as the magnitude of current at both frequencies.

The harmonic conversion loss of the transponder can be expressed as

$$L_h = 10 \log_{10} \left[\frac{R_{rad,0} |I_f|^2}{R_{rad,h} |I_h|^2} \right] \quad (6)$$

where I_f and I_h are the current amplitudes at f_0 and f_h , respectively. In this case, $I_f = 1.13 \text{ mA}$, $I_h = 0.15 \text{ mA}$, $R_{rad,0} = 4.46 \Omega$, and $R_{rad,h} = 89.98 \Omega$, which translates to a harmonic conversion loss of 4.5 dB. This value is governed by the power density incident upon the transponder, operating

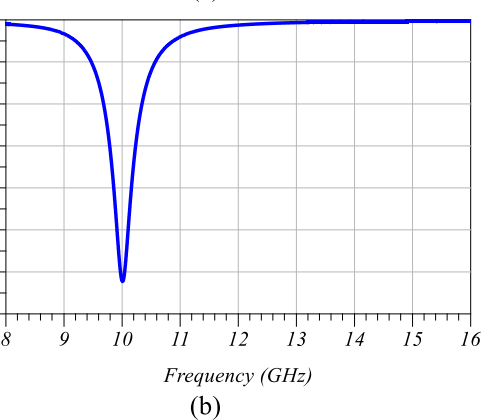
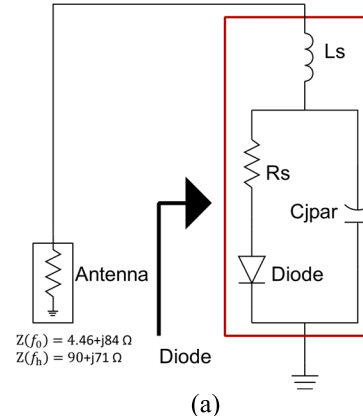


Fig. 3. Simulation of matching between dipole and diode (a) schematic, (b) reflection coefficient plot.

frequency, impedance matching between dipole and diode, as well as electrical specifications of diode. Specifically, the junction and parasitic capacitances of the diode significantly impact the achievable conversion loss—lower capacitances translate to lower conversion loss. Selecting a diode with low barrier junction is another necessity to ensure that a very low induced voltage can turn the diode on [24].

Finally, the received harmonic signal is scaled by the gain of transponder antenna, path loss, and radar receive antenna effective aperture at f_h . Table III summarizes each step in the harmonic radar transceiver link. In the examined case, a transmitted power of +22 dBm at 10 GHz translates to a received power of -66.4 dBm at 20 GHz.

IV. EXPERIMENTS AND DISCUSSION

A. Specifications of the Transponder

Fig. 5(a) shows the dimensions of the proposed transponder. The mass is reduced mainly by using thinner wire for the antenna. Although it is more prone to deformation, careful design can ensure transponder detectability is not sacrificed for mass reduction, as discussed in the next section.

Building this transponder does not require special tools—only a soldering iron with a very fine tip. A long wire is folded and soldered to the diode terminals at the desired locations, as shown in Fig. 5(b). Next, the wire is cut from each end to the desired length, which was achieved by adhering the transponder to a piece of paper with a printed ruler as depicted in Fig. 5(c). The diode used to make this transponder, the

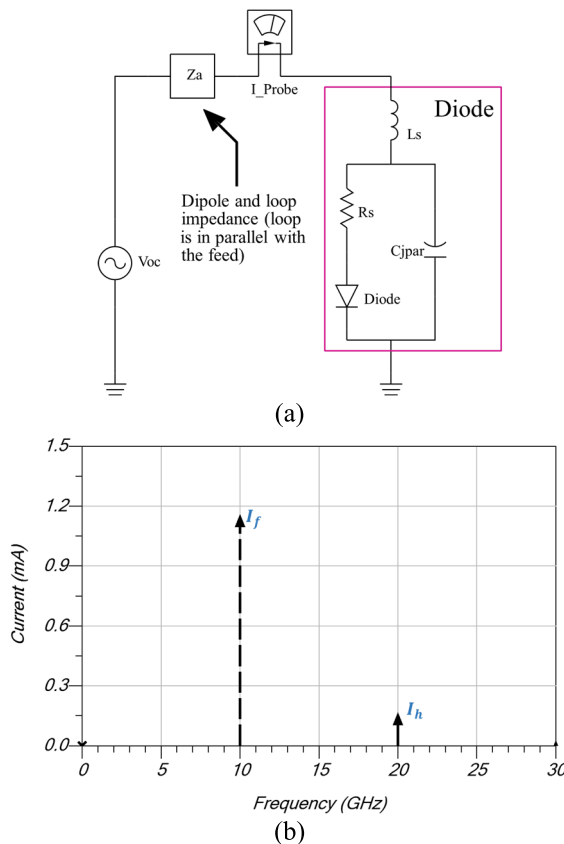


Fig. 4. The harmonic balance simulation (a) schematic (b) magnitude of the first and second current harmonics.

TABLE III
SUMMARY OF STEPS IN THE HARMONIC RADAR TRANSCEIVER LINK

Parameter	Value
TX power (f_0)	22 dBm
TX antenna gain (f_0)	15.8 dBi
Path loss (f_0)	60 dB
Transponder gain (f_0)	2.5 dBi
Mismatch loss (f_0)	0.25 dB
Harmonic conversion loss	4.5 dB
Transponder gain (f_h)	-0.45 dBi
Path loss (f_h)	66 dB
RX antenna gain (f_h)	24.5 dBi
RX power (f_h)	-66.4 dBm

MACOM MA4E2501L-1290, has dimensions of $0.6 \times 0.3 \times 0.15$ mm and, according to the datasheet, the junction potential of $V_j = 0.08$ V, a junction capacitance of 0.12 pF, dynamic resistance of 10Ω , and extremely low parasitic capacitance and inductance of 0.09 pF and 0.45 nH, respectively.

The antenna is made with AWG#44 wire, which is readily available in steel and copper. Although steel is sturdier and more durable, the strength of copper is acceptable for this application and preferred for ease of soldering. Considering the length and density of copper, the dipole weighs approximately $430 \mu\text{g}$. While the datasheet does not specify the diode's mass, it is estimated to be less than $70 \mu\text{g}$ based on its volume and the density of its dominant material, glass. Consequently, the transponder has a mass of nearly $500 \mu\text{g}$ which, to the

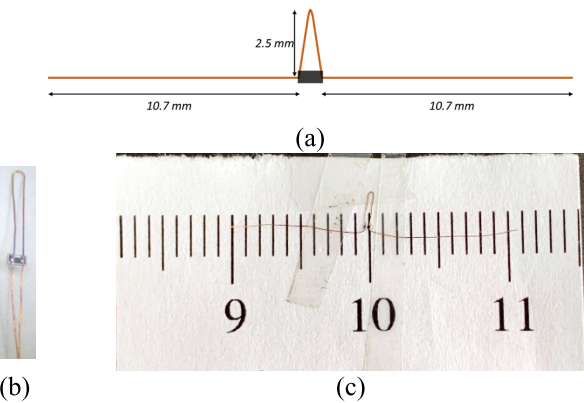


Fig. 5. Structure of transponder (a) dimensions, (b) loop and soldered diode, and (c) final transponder stuck on the scaled paper.

best of our knowledge, is the lightest available harmonic radar transponder.

In practice, attaching a transponder to an insect should be carefully evaluated on a case-by-case basis. While glue may be a feasible option that adds minimal mass, it is important to consider potential toxic interactions between certain adhesives and specific insect species.

B. Measurement of Transponder Broadside Harmonic Amplitude

The test setup to measure the transponder's broadside harmonic amplitude included an Agilent E8257C signal generator configured to produce a 10 GHz signal and an Agilent E4440A spectrum analyzer to capture the harmonic signal at 20 GHz. As shown in Fig. 6(a), a low-pass filter was used between the signal generator and transmitting antenna to suppress harmonics produced by the generator. The receiving antenna was directly connected to the spectrum analyzer without down-conversion or signal processing. To minimize power loss, cables were substituted with low-loss adapters for all connections. The power delivered to the transmit antenna port was measured to be $+22$ dBm and -90 dBm at f_0 and f_h , respectively. To maintain the desired orientation, the transponder was adhered to a piece of paper, which was in turn mounted on a piece of Styrofoam, as shown in Fig. 6(b). It is important to note that this mounting structure attenuates the received signal, especially if it is between radar and transponder. Fig. 6(c) shows the measurement setup in the anechoic test chamber.

Initially, the transponder antenna had a length of more than $2\lambda_0$. The wire was gradually trimmed from each end while the amplitude of the received harmonic was measured to find the optimal length. Cutting continued until the length was less than $0.5\lambda_0$. Transponders with unequal arm lengths, including a $2:1$ ratio, were considered; however, a length of $0.7\lambda_0$ with equal arms provided the maximum harmonic power. With the transponder placed 2.4 m from the radar antenna apertures, the power at the receive antenna port was measured to be approximately -70 dBm, which agrees with the simulation result of approximately -66.4 dBm.

There are several sources of measurement error. Calibration by connecting the signal generator directly to the spectrum analyzer was not possible because the transmitted and received

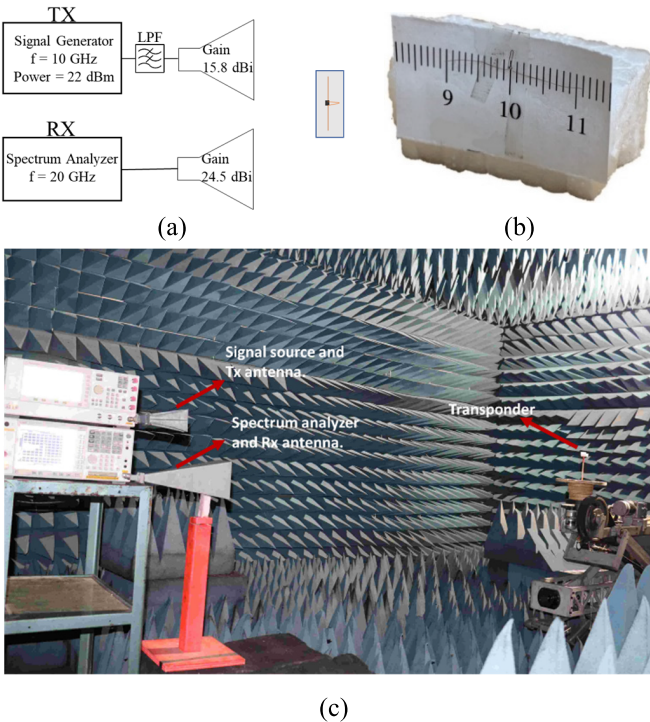


Fig. 6. Testing setup (a) diagram (b) a transponder mounted on styrofoam (c) measurement setup.

frequencies are different. As a result, the spectrum analyzer's power measurements at each frequency were assumed to be accurate. There may also be small error margins on the measured antenna gains. The transponder may not have been perfectly positioned in the direction of maximum gain for both radar antennas and may not have been perfectly broadside to the radar. The adaptors were assumed to exhibit negligible insertion loss. Finally, the transponder was hand-made, resulting in somewhat limited control over its dimensions.

C. Measuring Radiation Pattern

Although individually plotting the transponder's radiation pattern at f_0 and f_h is useful in the design stage, the summation of these patterns is more relevant to the overall performance of the transponder. Fig. 7 illustrates the setup for measuring this radiation pattern. The received signal at the harmonic frequency is measured using an Agilent N5242A PNA-X vector network analyzer (VNA). Since the transmitted and received signals are not at the same frequency, the VNA source port could not be used as the transmitter. Instead, an external signal generator was connected to the transmitting antenna, and the unused VNA port was match-terminated. To capture the radiation pattern, the receive antenna was connected to port 1 of VNA and S_{12} was measured while the transponder was rotated in the desired planes. Synchronization of the signal generator and VNA was achieved by connecting the signal generator's 10 MHz reference output to the VNA's external reference port. This allows the selection of a lower IF bandwidth within the VNA, which translates to a lower noise floor. Thus, the received harmonic signal was above the noise floor and easily detectable in most orientations. The associated

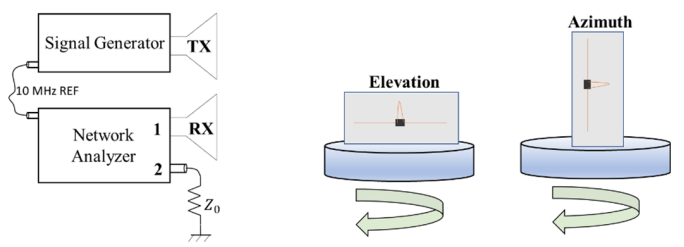


Fig. 7. Measurement of the transponder radiation pattern.

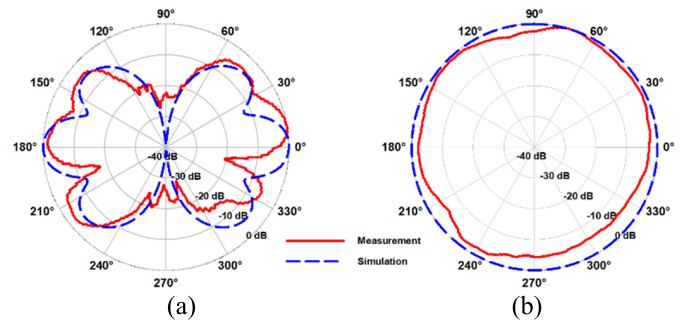


Fig. 8. Normalized radiation pattern of transponder in two planes (a) elevation (b) azimuth.

increase in sweep time can be accommodated by reducing the rotation speed or decreasing the angular resolution.

Fig. 8(a) and (b) show the normalized elevation- and azimuth-plane radiation patterns of the transponder as solid curves. The summation of fundamental and harmonic patterns obtained in simulation are added to these plots as dashed curves. The measured radiation pattern generally fits the summation of simulated patterns at f_0 and f_h . There are several reasons for the discrepancies. First, deep nulls are buried under the noise floor of the receiving instrument. In this measurement, the main lobe is roughly 25 dB higher than the minimum detectable signal. The mounting structure of the transponder affects both transmitted and radiated signals, especially when it is between the transponder and antennas. This effect is more considerable in the azimuth radiation pattern and caused up to 5 dB of loss in some directions. Although it would not be considered a measurement error, the insect's body would have a similar impact on the results. Finally, the transponder might be slightly misaligned or deformed compared to the simulated structure.

Because of the nonlinear behavior of the Schottky diode, characteristics such as its impedance and the corresponding harmonic magnitude are functions of the drive level. Therefore, the radiation pattern is expected to change slightly by changing the transmitted power, range, and relative orientation of the tag. However, the patterns have a similar shape regardless of incident power density, particularly the existence and locations of the main and side lobes. This was verified via radiation pattern measurements for transmitted powers of +22, +12, and +7 dBm as shown in Fig. 9. To reduce the noise floor at the power levels of +12 and +7 dBm, the IF bandwidth was set to 3 Hz, and the received harmonic was sampled at two-degree intervals. A lower transmitter power was also attempted, but the main lobes were not noticeably above the

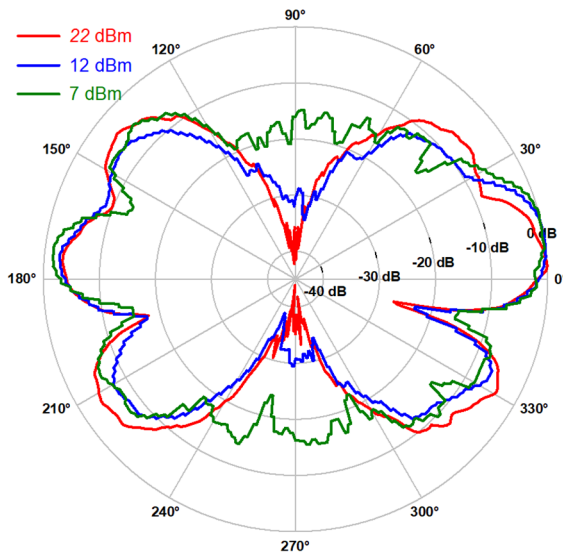


Fig. 9. Total radiation pattern measured at three different transmitted power levels.

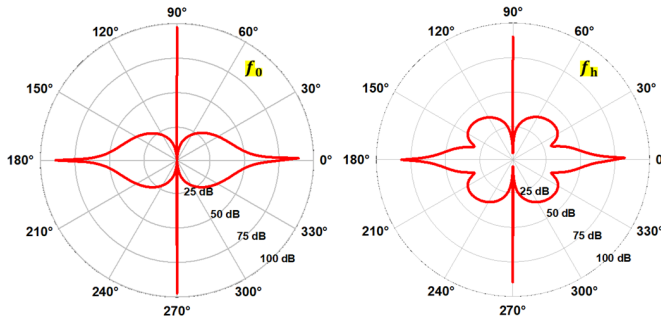


Fig. 10. Simulation result for the axial ratio at f_0 and f_h at the elevation plane.

noise level. These plots show a similar total radiation pattern over a power level range of 15 dB.

D. Transponder Axial Ratio

Since the dipole antenna used in this transponder is linearly polarized, a polarization mismatch between the transponder and radar will affect the power at both f_0 and f_h . Cross-polarization, therefore, results in an extremely low received harmonic signal. During measurements, a cross-polarized transponder was not detectable. Fig. 10 shows the axial ratio at frequencies of f_0 and f_h at the elevation plane. It shows that cross-polarization leads to signal losses of more than 40 dB in the main lobe at both frequencies—more than 80 dB in total. Circularly polarized radar antennas could be considered to maintain an uninterrupted received signal at the cost of maximum range and transponder mass.

The transponder is made with thin copper wire and is easily bent. While such bends in one or both dipole arms would not have a significant effect on the impedance match with the diode, the transponder radiation pattern would be affected [17]. However, a deformed transponder would also exhibit a smaller axial ratio, potentially improving performance under polarization mismatches.

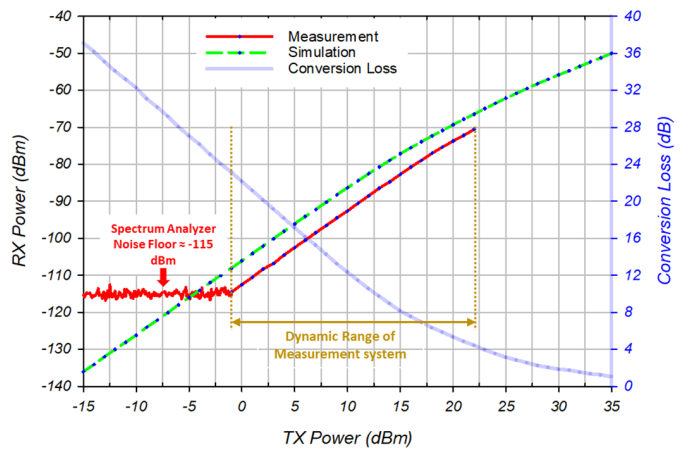


Fig. 11. Measured and simulated received power and simulated conversion loss versus the transmitted power for a constant range of 2.4 m.

E. Estimated Maximum Detection Range

It is important to note that the received signal was measured for a low power transmitter and short range. In practical harmonic radar systems, much higher transmit power is used to extend the detection range. Of course, the maximum detection range would be governed by both radar specifications and the performance of the transponder. There is a great deal of variation in the composition of harmonic radar systems, e.g., a portable system with lower gain antennas and limited transmit power versus a stationary system with large antenna and much more power. On the RX side, the minimum detectable signal has always been a problem for harmonic radar systems as they are limited by self-interference. A received harmonic signal as low as -100 dBm might be detectable if the dwell time on target is unlimited, but in practical cases it is much less sensitive. This encourages the application of advanced modulation and demodulation schemes to minimize the impact of self-interference.

To provide a better insight of the transponder performance under the different incident power densities or, equivalently, different radar ranges, the measured and simulated received power versus the transmitted power is plotted by sweeping the transmitter power as shown in Fig. 11. A plot of harmonic conversion loss is also shown, represented by a blue curve and referred to the right y-axis. The dynamic range of these measurements was limited by the maximum available power of the signal generator, $+22$ dBm, and the spectrum analyzer noise floor, -115 dBm. Results were obtained by reducing the signal generator power in 1-dB steps until the received power was no longer distinguishable from noise. Simulations were also performed for transmitted powers in the range of -15 to $+35$ dBm. The measurement and simulation plots are in an acceptable agreement with a maximum error of 6 dB, which was justified earlier in Section IV-B. The slope of the measurement plot is approximately 2 and the simulation plot has the slope of approximately 2 over the measurement range, reducing to approximately 1 for higher transmitted powers. The slope at lower transmitted power agrees with the findings in [25].

The link analysis presented above can be applied to a practical radar system, such as the one described in [11],

to estimate a practical detection range. The radar includes a TX power of 25 kW and TX and RX antenna gains of 28.5 and 27.4 dBi, respectively. The received power with the transponder presented here is in the range of -70 and -90 dBm at distances of 150 to 450 m, which is enough for detection with an acceptable false alarm probability based on the noise floor and signal to noise ratio of the receiver.

V. CONCLUSION

A harmonic radar transponder was constructed with copper wire having a AWG#44 and a Schottky diode with a footprint of 0201 to reach a total mass of less than $500\ \mu\text{g}$. To our knowledge, this is the lightest available harmonic radar transponder. Construction is relatively easy as it requires soldering a diode to a wire and then cutting the wire to the proper length. Transponder performance in terms of harmonic conversion efficiency has not been sacrificed by mass or structure. According to simulations, an available power of approximately -20 dBm led to a conversion loss of 4.5 dB. Measurements performed in an anechoic chamber under similar conditions confirmed these results. The simulation predicted that a TX power of $+22$ dBm and a range of 2.4 m resulted in a received power of -66.4 dBm at the harmonic, which agreed well with the measured result of -70 dBm. The transponder's radiation pattern was measured with a new method: instead of measuring the transponder's radiation pattern at the first and second harmonics using the intermodulation technique, the total radiation pattern was measured by employing an external signal generator that was synchronized with a network analyzer acting as a receiver. The measured pattern was in good agreement with the simulation. This transponder will enable the tracking of insects that are far too small to support the state-of-the-art radio transmitters. For future advancements in this area, it will be important to further investigate the mechanical robustness of the transponder.

ACKNOWLEDGMENT

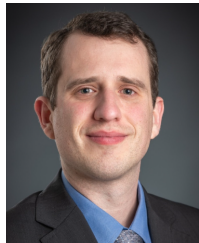
The authors would like to acknowledge CMC Microsystems for the provision of products and services that facilitated this research, including Keysight Technologies PathWave Software Platform.

REFERENCES

- [1] A. Mishra and C. Li, "A review: Recent progress in the design and development of nonlinear radars," *Remote Sens.*, vol. 13, no. 24, p. 4982, Dec. 2021, doi: [10.3390/RS13244982](https://doi.org/10.3390/RS13244982).
- [2] P. Nallabolu, L. Zhang, H. Hong, and C. Li, "Human presence sensing and gesture recognition for smart home applications with moving and stationary clutter suppression using a 60-GHz digital beamforming FMCW radar," *IEEE Access*, vol. 9, pp. 72857–72866, 2021, doi: [10.1109/ACCESS.2021.3080655](https://doi.org/10.1109/ACCESS.2021.3080655).
- [3] E. T. Cant, A. D. Smith, D. R. Reynolds, and J. L. Osborne, "Tracking butterfly flight paths across the landscape with harmonic radar," *Proc. Roy. Soc. B. Biol. Sci.*, vol. 272, no. 1565, pp. 785–790, Apr. 2005, doi: [10.1098/RSPB.2004.3002](https://doi.org/10.1098/RSPB.2004.3002).
- [4] S. Lioy et al., "Tracking the invasive hornet *Vespa velutina* in complex environments by means of a harmonic radar," *Sci. Rep.*, vol. 11, no. 1, pp. 1–10, Jun. 2021, doi: [10.1038/s41598-021-91541-4](https://doi.org/10.1038/s41598-021-91541-4).
- [5] E. A. Capaldi et al., "Ontogeny of orientation flight in the honeybee revealed by harmonic radar," *Nature*, vol. 403, no. 6769, pp. 537–540, Feb. 2000, doi: [10.1038/35000564](https://doi.org/10.1038/35000564).
- [6] N. D. Miller, T. J. Yoder, N. C. Manoukis, L. A. F. N. Carvalho, and M. S. Siderhurst, "Harmonic radar tracking of individual melon flies, *Zeugodacus cucurbitae*, in Hawaii: Determining movement parameters in cage and field settings," *PLoS ONE*, vol. 17, no. 11, Nov. 2022, Art. no. e0276987, doi: [10.1371/JOURNAL.PONE.0276987](https://doi.org/10.1371/JOURNAL.PONE.0276987).
- [7] F. Meloche and P. M. Albert, "A lighter transponder for harmonic radar," in *Proc. Eur. Radar Conf.*, Sep. 2006, pp. 233–236, doi: [10.1109/EURAD.2006.280317](https://doi.org/10.1109/EURAD.2006.280317).
- [8] B. G. Colpitts and G. Boiteau, "Harmonic radar transceiver design: Miniature tags for insect tracking," *IEEE Trans. Antennas Propag.*, vol. 52, no. 11, pp. 2825–2832, Nov. 2004, doi: [10.1109/TAP.2004.835166](https://doi.org/10.1109/TAP.2004.835166).
- [9] Z. Tsai et al., "A high-range-accuracy and high-sensitivity harmonic radar using pulse pseudorandom code for bee searching," *IEEE Trans. Microw. Theory Techn.*, vol. 61, no. 1, pp. 666–675, Jan. 2013, doi: [10.1109/TMTT.2012.2230020](https://doi.org/10.1109/TMTT.2012.2230020).
- [10] J. Kiriazi, J. Nakakura, K. Hall, N. Hafner, and V. Lubecke, "Low profile harmonic radar transponder for tracking small endangered species," in *Proc. 29th Annu. Int. Conf. IEEE Eng. Med. Biol. Soc.*, Aug. 2007, pp. 2338–2341, doi: [10.1109/IEMB.2007.4352795](https://doi.org/10.1109/IEMB.2007.4352795).
- [11] D. Milanesio, M. Saccani, R. Maggiore, D. Laurino, and M. Porporato, "Design of an harmonic radar for the tracking of the Asian yellow-legged hornet," *Ecol. Evol.*, vol. 6, no. 7, pp. 2170–2178, Apr. 2016, doi: [10.1002/ECE3.2011](https://doi.org/10.1002/ECE3.2011).
- [12] R. Ala and B. G. Colpitts, "Development of extra low mass harmonic radar transponders," in *Proc. IEEE 19th Int. Symp. Antenna Technol. Appl. Electromagn. (ANTEM)*, Aug. 2021, pp. 1–2, doi: [10.1109/ANTEM51107.2021.9518747](https://doi.org/10.1109/ANTEM51107.2021.9518747).
- [13] K. Rasilainen, J. Ilvonen, A. Lehtovuori, J. Hannula, and V. Viikari, "On design and evaluation of harmonic transponders," *IEEE Trans. Antennas Propag.*, vol. 63, no. 1, pp. 15–23, Jan. 2015, doi: [10.1109/TAP.2014.2366193](https://doi.org/10.1109/TAP.2014.2366193).
- [14] X. Gu, N. N. Srinaga, L. Guo, S. Hemour, and K. Wu, "Diplexer-based fully passive harmonic transponder for sub-6-GHz 5G-compatible IoT applications," *IEEE Trans. Microw. Theory Techn.*, vol. 67, no. 5, pp. 1675–1687, May 2019, doi: [10.1109/TMTT.2018.2883979](https://doi.org/10.1109/TMTT.2018.2883979).
- [15] A. Lavrenko and J. Cavers, "Two-region model for harmonic radar transponders," *Electron. Lett.*, vol. 56, no. 16, pp. 835–838, Aug. 2020, doi: [10.1049/EL.2020.0779](https://doi.org/10.1049/EL.2020.0779).
- [16] H. Aumann, E. Kus, B. Cline, and N. W. Emanetoglu, "An asymmetrical dipole tag with optimum harmonic conversion efficiency," in *Proc. IEEE Int. Symp. Antennas Propag.*, Jul. 2012, pp. 1–2, doi: [10.1109/APS.2012.6348447](https://doi.org/10.1109/APS.2012.6348447).
- [17] R. Ala, B. G. Colpitts, and N. Kozma, "Evaluation and improvement of the performance of harmonic RADAR transponders," in *Proc. IEEE Int. Radar Conf. (RADAR)*, Apr. 2020, pp. 659–664, doi: [10.1109/RADAR42522.2020.9114545](https://doi.org/10.1109/RADAR42522.2020.9114545).
- [18] M. Ritamaki, A. Ruhanen, V. Kukko, J. Miettinen, and L. H. Turner, "Contactless radiation pattern measurement method for UHF RFID transponders," *Electron. Lett.*, vol. 41, no. 13, pp. 723–724, Jun. 2005, doi: [10.1049/EL:20051029](https://doi.org/10.1049/EL:20051029).
- [19] K. Rasilainen and V. V. Viikari, "Transponder designs for harmonic radar applications," *Int. J. Antennas Propag.*, vol. 2015, pp. 1–9, Jan. 2015, doi: [10.1155/2015/565734](https://doi.org/10.1155/2015/565734).
- [20] G. Storz and A. Lavrenko, "Compact low-cost FMCW harmonic radar for short range insect tracking," in *Proc. IEEE Int. Radar Conf. (RADAR)*, Washington, DC, USA, Apr. 2020, pp. 642–647, doi: [10.1109/RADAR42522.2020.9114612](https://doi.org/10.1109/RADAR42522.2020.9114612).
- [21] K. Rasilainen, J. Ilvonen, J. Hannula, and V. Viikari, "Designing harmonic transponders using lumped-component matching circuits," *IEEE Antennas Wireless Propag. Lett.*, vol. 16, pp. 246–249, 2017, doi: [10.1109/LAWP.2016.2570938](https://doi.org/10.1109/LAWP.2016.2570938).
- [22] A. Lavrenko, B. Litchfield, G. Woodward, and S. Pawson, "Design and evaluation of a compact harmonic transponder for insect tracking," *IEEE Microw. Wireless Compon. Lett.*, vol. 30, no. 4, pp. 445–448, Apr. 2020, doi: [10.1109/LMWC.2020.2972744](https://doi.org/10.1109/LMWC.2020.2972744).
- [23] K. Gallagher, R. Narayanan, G. Mazzaro, A. Martone, and K. Sherbondy, "Static and moving target imaging using harmonic radar," *Electronics*, vol. 6, no. 2, p. 30, Apr. 2017, doi: [10.3390/electronics6020030](https://doi.org/10.3390/electronics6020030).
- [24] J. R. Riley and A. D. Smith, "Design considerations for an harmonic radar to investigate the flight of insects at low altitude," *Comput. Electron. Agricult.*, vol. 35, nos. 2–3, pp. 151–169, Aug. 2002, doi: [10.1016/S0168-1699\(02\)00016-9](https://doi.org/10.1016/S0168-1699(02)00016-9).
- [25] M. A. Merlini, A. G. B. Colpitts, S. Gill, B. G. Colpitts, and B. R. Petersen, "Channel modelling and efficient time-domain simulation of a harmonic transponder tag," in *Proc. 6th Int. Conf. Telecommun. Remote Sens.*, Nov. 2017, pp. 43–47.



Ramin Ala received the B.Sc. degree in electrical engineering from the University of Isfahan, Isfahan, Iran, in 2007, and the M.Sc. degree in electrical engineering from the K. N. Toosi University of Technology, Tehran, Iran, in 2010. He is currently pursuing the Ph.D. degree in electrical engineering with the University of New Brunswick, Canada. His research focuses on microwave engineering and radar, including the design of passive and active devices and antennas.



Chris D. Rouse (Member, IEEE) received the B.Sc.E. and Ph.D. degrees in electrical engineering from the University of New Brunswick (UNB) in 2009 and 2014, respectively. From 2014 to 2016, he pursued an Industrial Research and Development Fellowship with Seamatica Aerospace (St. John's, NL). In 2016, he joined Solace Power (Mount Pearl, NL) as a Senior Electrical Researcher and was promoted to RF Team Lead in 2020. Later that year, he joined the Directorate of Regulatory Standards within Innovation, Science and Economic Development Canada (Ottawa, ON) as a Senior Spectrum Engineer. He is currently an Assistant Professor with the Department of Electrical and Computer Engineering, UNB, where his research focuses on near-field wireless power transfer, RF exposure analysis, and radar.

Bruce G. Colpitts (Senior Member, IEEE) received the B.Sc.E., M.Sc.E., and Ph.D. degrees in electrical engineering from the University of New Brunswick, Fredericton, NB, Canada, in 1983, 1985, and 1988, respectively. In 1989, he joined the Department of Electrical and Computer Engineering, University of New Brunswick, where he is currently a Professor. He is a registered Professional Engineer in the Province of New Brunswick, Canada. He coordinated the implementation of the Optical Fiber Systems Laboratory, which has hosted different advanced research projects in the areas of fiber optic sensor development, electromagnetic systems, and communications. His research interests are primarily related to microwave circuits, antennas, and propagation; including measurement, simulation, hardware development, and application. Recent research projects include harmonic radar design, optical strain and temperature sensing, MRI investigations, and numerous antenna designs.